Unleashing the Power of Cobalt Pyroborate: Superior Performance in Sulfate Radical Advanced Oxidation Processes

En-Xuan Lin, Fang-Yu Wu, Yu-Lun Zhu, Yu-Rong Chang, Po-Yi Wu, **Pei Yuin Keng***

Department of Materials Science and Engineering, National Tsing Hua University, Hsinchu 30013, Taiwan

* Corresponding author. Tel.: +886-3-5715131 ext. 33884; fax: +886-3-5722366; e-mail address: keng.py@gapp.nthu.edu.tw (P.Y.K).

Table 1 Comparative analysis of Co_3O_4 heterostructures in previous studies relative to the current work. Abbreviations for organic pollutants: 4-NP signifies 4-nitrophenol; BPA stands for bisphenol-A; PNT represents phenacetin; SDZ denotes sulfadiazine; RhB refers to Rhodamine-B; SMZ is for sulfamethoxazole; SSZ indicates sulfasalazine; CBZ is an abbreviation for carbamazepine; and TC designates tetracycline.

Catalyst	Pollutant	Reaction conditions	Performance	Reference
Co_3O_4 nanoparticles and N-functionalized carbon nanosheet frameworks (Co_3O_4-NCNF)	4-NP	[PMS] = 3 mM; catalyst = 0.14 g/L; [4-NP] = 20 ppm; time = 60 mins	100.0% $k = 0.137\ min^{-1}$	[1]
Ultrafine Co_3O_4 incorporated carbon composites (Co_3O_4/CC)	BPA	[PMS] = 0.66 mM; catalyst = 0.1 g/L; [BPA] = 10 ppm; time = 10 mins	97% $k = 0.45\ min^{-1}$	[2]
Two-dimensional (2D) ultrathin perforated Co_3O_4 nanosheet	BPA	[PMS] = 0.25 mM; catalyst = 0.05 g/L; [SMZ] = 10 ppm; time = 30 mins	98.0% $k = 0.112\ min^{-1}$	[3]

Co_3O_4 anchored on biochar derived from chitosan (Co_3O_4@BCC)	PNT	[PMS] = 1.0 mM; catalyst = 0.05 g/L; [PNT] = 10 ppm; time = 15 mins	100.0% $k = 0.32\ min^{-1}$	[4]
Co_3O_4-MnO_2 nanoparticles moored on biochar (Co_3O_4-MnO_2/BC)	SDZ	[PMS] = 1.0 mM; catalyst = 0.1 g/L; [SDZ] = 25 ppm; time = 10 mins	100.0% $k = 0.482\ min^{-1}$	[5]
Cobalt@porous carbon nanosheets	4-NP	[PMS] = 3.9 mM; catalyst = 0.16 g/L; [4-NP] = 20 ppm; time = 12 mins	99.5% $k = 0.618\ min^{-1}$	[6]
Co-doped g-C_3N_4	RhB	[PMS] = 0.12 mM; catalyst = 0.4 g/L; [RhB] = 10 ppm; time = 25 mins	99% $k = 0.2208\ min^{-1}$	[7]
C_3N_5-$Co_{0.59}$	SMX	[PMS] = 1.0 mM; catalyst = 0.5 g/L; [SMX] = 10 ppm; time = 20 mins	99.57% $k = 0.3515\ min^{-1}$	[8]
In situ N-doped carbon-coated mulberry-like cobalt manganese oxide (HCoMnOx@NC)	SMZ, SSZ, CBZ, etc.	[PMS] = 0.3 mM; catalyst = 0.1 g/L; [pollutant] = 30μM; time = 30 mins	100% : SSZ, CBZ 95.4% SMZ $k_{SMZ} = 0.0867\ min^{-1}$ $k_{SSZ} = 0.1769\ min^{-1}$ $k_{CBZ} = 0.5069\ min^{-1}$	[5]
cobalt sulfide-reduced graphene oxide nanocomposite (CoS-rGO)	RhB	[PMS] = 0.05 mM; catalyst = 0.25 g/L; [RhB] = 30 μM; time = 8 mins	100% $k = 0.6714\ min^{-1}$	[9]
Our work $Co_2B_2O_5$	TC, 4-NP, SMX	[PMS] = 1 mM; catalyst = 0.12 g/L [SMX] = 10 ppm [TC] = 50 ppm [4-NP] = 40 ppm	95.2% SMX $k_{SMX} = 0.092\ min^{-1}$ 97.9% TC $k_{TC} = 0.16\ min^{-1}$ 96.8% 4-NP $k_{4NP} = 0.12\ min^{-1}$	Our work

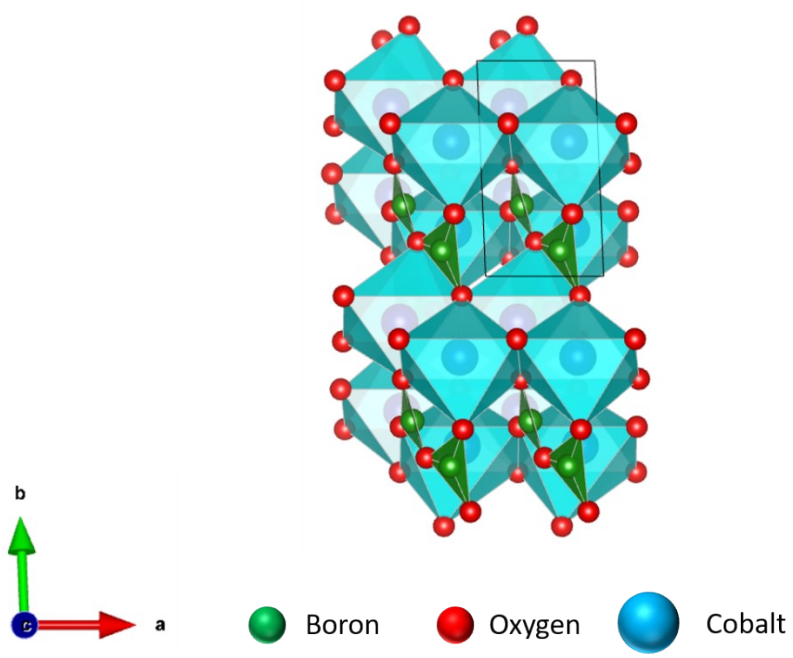

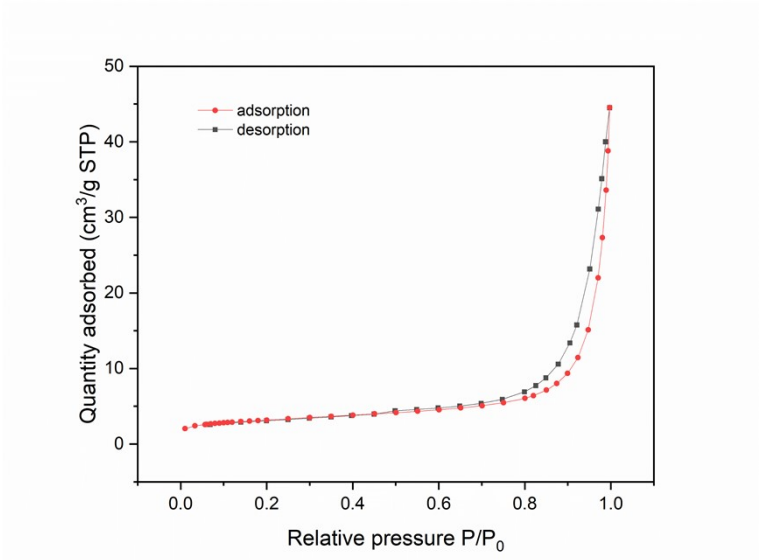

Figure S1. Crystal structure of cobalt pyroborate

Figure S2: BET isotherms using N_2 at 77 K of $Co_2B_2O_5$

The Fourier Transform Infrared (FTIR) spectrum of $Co_2B_2O_5$ is presented (Fig. 4), revealing several characteristic absorption bands associated with cobalt, boron and oxygen. Notably, several peaks have been identified, including the O-H vibration at 3425.88 cm^{-1}, as well as the asymmetric

B-O stretching peaks of the three-coordinate boron at 1465.58 cm^{-1} and 1273.52 cm^{-1}, and of four-coordinate boron at 1170.05 cm^{-1} and 1012.5 cm^{-1}.[10,11] The symmetric B-O stretching vibration of the four-coordinate boron is evident at 906 cm^{-1} and 820.88 cm^{-1}, while the symmetric stretching vibrations of the four-coordinate boron group emerged at 872 cm^{-1}.[10,11] Additionally, the absorbance band at 768 cm-1 can be assigned to the oxygen bridge of one tetrahedral and one tetragonal boron group.[10,11] The Co-O bond is represented by the absorption peaks at 595.50 cm^{-1} and 662.50 cm^{-1}, and the absorbance band at 697.03 cm^{-1} is due to the O-B-O bonding.[12–15] Our FTIR results is commensurate with the XPS and XRD analyses, which confirms the structural characteristic of $Co_2B_2O_5$.

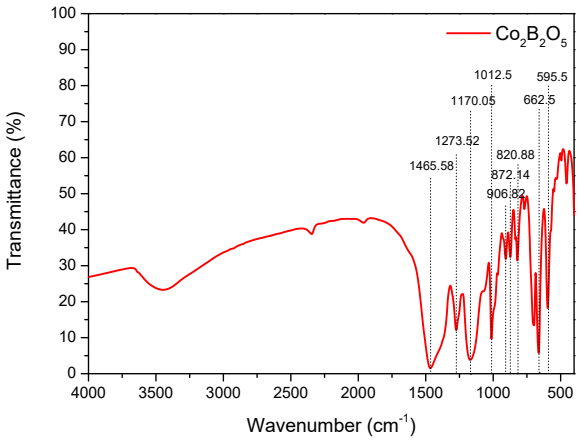

Figure S3: FTIR spectrum of $Co_2B_2O_5$ nanoparticle

ICP-MS

The ICP-MS analysis of the $Co_2B_2O_5$ revealed the elemental composition of Co:B weight ratio to 0.529:0.151, which is commensurate with the theoretical value of 0.536:0.1(Table S1). The higher proportion of boron than the ideal value may be due to the residual portion of boric acid during synthesis.

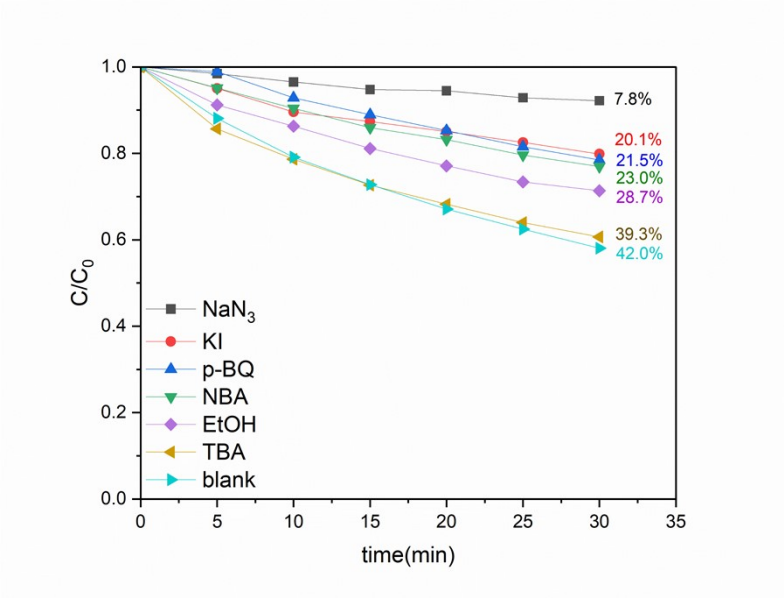

Figure S3: Kinetic plot of trapping experiment using CoO as a catalyst in SR-AOPs. Reaction conditions: $[4\text{-NP}]_0$ = 40 ppm; [catalyst] = 125 mg/L; [PMS] = 1 mM; [trapping agent] = 1 mM.

Table S2 ICP-MS result of the pristine $Co_2B_2O_5$ nanoparticles and the solution after a standard SR-AOPs degradation reaction using $Co_2B_2O_5$ as catalyst

Element/Concentration / Sample	Co	B
$Co_2B_2O_5$ (ppm)	71.50	20.71
Weight percent in catalyst (%)	52.9	15.1
Co and B leached in the solution (ppm)	21.22	7.715

Table S3 Relative atomic percentage of Co^{2+} and Co^{3+} in pristine versus spent $Co_2B_2O_5$

Elements in different chemical states	Relative contents (at. %)	
	Pristine	Spent
Co^{2+}	39.8	61.3
Co^{3+}	60.2	38.7

References

[1] G. Yi, M. Ye, J. Wu, Y. Wang, Y. Long, G. Fan, Facile chemical blowing synthesis of interconnected N-doped carbon nanosheets coupled with Co3O4 nanoparticles as superior peroxymonosulfate activators for p-nitrophenol destruction: Mechanisms and degradation pathways, Appl. Surf. Sci. 593 (2022) 153244. https://doi.org/10.1016/j.apsusc.2022.153244.

[2] R. Luo, C. Liu, J. Li, C. Wang, X. Sun, J. Shen, W. Han, L. Wang, Convenient synthesis and engineering of ultrafine Co3O4-incorporated carbon composite: towards practical application of environmental remediation, J. Mater. Chem. A 6 (2018) 3454–3461. https://doi.org/10.1039/C7TA11052A.

[3] Q. Wang, Z. Xu, Y. Cao, Y. Chen, X. Du, Y. Yang, Z. Wang, Two-dimensional ultrathin perforated Co3O4 nanosheets enhanced PMS-Activated selective oxidation of organic micropollutants in environmental remediation, Chem. Eng. J. 427 (2022) 131953. https://doi.org/10.1016/j.cej.2021.131953.

[4] J. Zhou, X. Yang, Q. Wei, Y. Lan, J. Guo, Co3O4 anchored on biochar derived from chitosan (Co3O4@BCC) as a catalyst to efficiently activate peroxymonosulfate (PMS) for degradation of phenacetin, J. Environ. Manage. 327 (2023) 116895. https://doi.org/10.1016/j.jenvman.2022.116895.

[5] A. Wang, Y. Chen, Z. Zheng, H. Wang, X. Li, Z. Yang, R. Qiu, K. Yan, In situ N-doped carbon-coated mulberry-like cobalt manganese oxide boosting for visible light driving photocatalytic degradation of pharmaceutical pollutants, Chem. Eng. J. 411 (2021) 128497. https://doi.org/10.1016/j.cej.2021.128497.

[6] L. Hu, X. Liu, A. Guo, J. Wu, Y. Wang, Y. Long, G. Fan, Cobalt with porous carbon architecture: Towards of 4-nitrophenol degradation and reduction, Sep. Purif. Technol. 288 (2022) 120595. https://doi.org/10.1016/j.seppur.2022.120595.

[7] L. Wang, X. Guo, Y. Chen, S. Ai, H. Ding, Cobalt-doped g-C3N4 as a heterogeneous catalyst for photo-assisted activation of peroxymonosulfate for the degradation of organic contaminants, Appl. Surf. Sci. 467–468 (2019) 954–962. https://doi.org/10.1016/j.apsusc.2018.10.262.

[8] P. He, C. Gu, B. Tang, Y. Zhou, M. Gan, J. Zhu, Expeditious degradation of SMX by high-valent cobalt-oxo species derived from cobalt-doped C3N5-activated peroxymonosulfate with the assistance of visible light, Sep. Purif. Technol. 301 (2022) 122009. https://doi.org/10.1016/j.seppur.2022.122009.

[9] L. Amirache, F. Barka-Bouaifel, P. Borthakur, M.R. Das, H. Ahouari, H. Vezin, A. Barras,

B. Ouddane, S. Szunerits, R. Boukherroub, Cobalt sulfide-reduced graphene oxide: An efficient catalyst for the degradation of rhodamine B and pentachlorophenol using peroxymonosulfate, J. Environ. Chem. Eng. 9 (2021) 106018. https://doi.org/10.1016/j.jece.2021.106018.

[10] A.M. Abdelghany, F.H. ElBatal, H.A. ElBatal, F.M. EzzElDin, Optical and FTIR structural studies of CoO-doped sodium borate, sodium silicate and sodium phosphate glasses and effects of gamma irradiation-a comparative study, J. Mol. Struct. 1074 (2014) 503–510. https://doi.org/10.1016/j.molstruc.2014.06.011.

[11] A.S. Kipcak, M. Yildirim, S. Aydin Yuksel, E. Moroydor Derun, S. Piskin, The Synthesis and Physical Properties of Magnesium Borate Mineral of Admontite Synthesized from Sodium Borates, Adv. Mater. Sci. Eng. 2014 (2014) 1–9. https://doi.org/10.1155/2014/819745.

[12] O.Y. Gumus, H.I. Unal, O. Erol, B. Sari, Synthesis, characterization, and colloidal properties of polythiophene/borax conducting composite, Polym. Compos. 32 (2011) 418–426. https://doi.org/10.1002/pc.21057.

[13] H.T. Jang, E.M. Jung, S.H. Park, P. Hemalatha, Synthesis and Characterization of CoO-ZnO Catalyst System for Selective CO Oxidation, Int. J. Control Autom. 6 (2013) 31–40. https://doi.org/10.14257/ijca.2013.6.6.04.

[14] S.Z. Mohammadi, B. Lashkari, A. Khosravan, Green synthesis of Co3O4 nanoparticles by using walnut green skin extract as a reducing agent by using response surface methodology, Surf. Interfaces 23 (2021) 100970. https://doi.org/10.1016/j.surfin.2021.100970.

[15] V. Sankar Devi, M. Athika, E. Duraisamy, A. Prasath, A. Selva Sharma, P. Elumalai, Facile sol-gel derived nanostructured spinel Co3O4 as electrode material for high-performance supercapattery and lithium-ion storage, J. Energy Storage 25 (2019) 100815. https://doi.org/10.1016/j.est.2019.100815.